

Article

Correlation between Ground ^{222}Rn and ^{226}Ra and Long-Term Risk Assessment at the at the Bauxite Bearing Area of Fongo-Tongo, Western Cameroon

Léonard Boris Djeufack ^{1,2}, Guillaume Samuel Bineng ¹, Oumar Bobbo Modibo ² ,
Joseph Emmanuel Ndjana Nkoulou II ² and Saïdou ^{1,2,*} 

¹ Nuclear Physics Laboratory, Faculty of Science, University of Yaoundé I, Yaoundé P.O. Box 812, Cameroon

² Research Centre for Nuclear Science and Technology, Institute of Geological and Mining Research (IRGM), Yaoundé P.O. Box 4110, Cameroon

* Correspondence: saidous2002@yahoo.fr; Tel.: +237-674-174-473

Simple Summary: This paper presents a study of radioactivity in soil that included an assessment of radiological risk parameters and long-term health risks from exposure to naturally occurring radionuclides in soil at the bauxite-bearing area of Fongo-Tongo in Western Cameroon. The radionuclides measured in the soil had concentration values above the recommended limits. However, the total long-term excess risk at the site decreased progressively over the years, and the maximum value of 8.58×10^{-3} was obtained at $T = 0$ years. In addition, the external pathway is the largest contributor to the total excess risk assessed inside the building. The maximum risk value for this pathway, which is 2.33×10^{-2} , was obtained at $T = 30$ years before decreasing sharply thereafter.



Citation: Djeufack, L.B.; Bineng, G.S.; Modibo, O.B.; Ndjana Nkoulou, J.E., II; Saïdou. Correlation between Ground ^{222}Rn and ^{226}Ra and Long-Term Risk Assessment at the at the Bauxite Bearing Area of Fongo-Tongo, Western Cameroon. *Radiation* **2022**, *2*, 387–404. <https://doi.org/10.3390/radiation2040029>

Academic Editor: Michele Guida

Received: 9 October 2022

Accepted: 9 November 2022

Published: 14 November 2022

Publisher's Note: MDPI stays neutral with regard to jurisdictional claims in published maps and institutional affiliations.

Abstract: The aim of the current work was to study natural radioactivity in soil and the correlation between ^{222}Rn and ^{226}Ra in the ground and to assess the onsite and indoor long-term excess cancer risk at the bauxite bearing area of Fongo-Tongo in Western Cameroon. ^{222}Rn was measured in the ground at a depth of one meter, using Markus 10 detector. ^{226}Ra , ^{232}Th , and ^{40}K activity concentrations were measured in soil by two techniques, in situ and laboratory gamma spectrometry. The mean values of ^{222}Rn concentrations in the ground were $69 \pm 18 \text{ kBq m}^{-3}$ for Fongo-Tongo and $82 \pm 34 \text{ kBq m}^{-3}$ for the locality of Dschang, respectively. The mean values of ^{226}Ra , ^{232}Th , and ^{40}K activity concentrations obtained with in situ gamma spectrometry were 129 ± 22 , 205 ± 61 , and $224 \pm 39 \text{ Bq kg}^{-1}$ for ^{226}Ra , ^{232}Th , and ^{40}K , respectively, and those obtained by laboratory gamma spectrometry were 129 ± 23 , 184 ± 54 , and $237 \pm 44 \text{ Bq kg}^{-1}$, respectively. A strong correlation between ^{222}Rn and ^{226}Ra activity concentrations determined by in situ and laboratory measurements ($R^2 = 0.86$ and 0.88 , respectively) was found. In addition, it is shown that the total excess cancer risk has a maximum value of 8.6×10^{-3} at $T = 0$ year and decreases progressively in the long term. It is also shown that ^{226}Ra makes a major contribution, i.e., above 70%, to the total excess cancer risk.

Keywords: radium-226; radon-222; life excess cancer risk



Copyright: © 2022 by the authors. Licensee MDPI, Basel, Switzerland. This article is an open access article distributed under the terms and conditions of the Creative Commons Attribution (CC BY) license (<https://creativecommons.org/licenses/by/4.0/>).

1. Introduction

Areas with high mining potential generally represent a very interesting field for environmental monitoring before, during, and after mining. In the case of the sites hosting not-yet-exploited ore deposits, activities related to exploration led to the transfer of soil from underground to the ground surface. This action could lead to the environmental pollution by natural radioactive materials, increasing the exposure level of inhabitants to natural radiation. Moreover, human exposure to natural radiation sources is ubiquitous and inescapable. Radionuclides in the earth's crust vary from one environment to another, depending on the soil and geological profile [1]. The content and type of radioelement depend, therefore, on the bedrock [2–4]. A long exposure to the natural radionuclides

(^{226}Ra , ^{232}Th , and ^{40}K) is mainly responsible for some cancers and sometimes for the effects of genetic mutations. They constitute a real threat to human health [5–7].

Many investigations on natural radioactivity have been made in the world [8–10]. The investigation conducted in Cameroon revealed the occurrence of high levels of radioactivity in some specific areas of the country [11–13]. These high radioactivity levels are more localized in areas with uranium, thorium, and bauxite mining potential. It is the case of the natural radioactivity measurements made in Poli and Lolodorf, Douala, Fongo-Tongo, Dschang, and Ngaoundal [13–15]. They revealed high ^{238}U , ^{232}Th , and ^{40}K activity concentrations in soil compared to their corresponding world levels, as well as ^{222}Rn and ^{220}Rn concentrations in dwellings above the WHO reference level [12,16–18]. These mentioned studies showed that the ^{222}Rn level in homes depends considerably on the type of architecture, geological structure, and mineralogical composition of soil of the area [16,19]. A good correlation between ^{238}U and ^{232}Th activity concentrations in soil with ^{222}Rn and ^{220}Rn in dwellings was found in the areas, respectively [20,21].

However, these studies have not specifically examined the correlation that may exist between ^{222}Rn and ^{226}Ra activity concentrations in soil. ^{222}Rn is a direct progeny of ^{226}Ra [1]. Therefore, its concentration in soil should be proportional to that of the direct parent, ^{226}Ra . ^{222}Rn measurement was performed by using a MARKUS 10 detector to a depth of 1 m in the ground. The determination of the activity concentrations of ^{226}Ra , ^{232}Th , and ^{40}K in soil was performed with a NaI (TI) gamma spectrometer. In addition, the ^{222}Rn and ^{226}Ra activity concentrations determined by in situ and laboratory measurements are strongly correlated, and these correlation coefficients were determined. Radiological parameters (AEED, Ra_{eq} , H_{in} , H_{ex} , ELCR, I_{γ} , and I_{α}) were determined to assess the level of public exposure to natural radioactivity in the area, and a map of the distribution of ^{226}Ra and ^{222}Rn concentrations in soil was established.

2. Materials and Methods

2.1. Study Areas

The area is located on the mountainous chain region of the Western Cameroon, specifically at the southwestern flanks of the Bamboutos Mountains [22]. The climate of the area is sub-equatorial, Cameroonian type, cold and humid, characterized by a long rainy season (March–November) and a short dry season (December–February). The average temperature and rainfall in the area are 22.5 °C and 1364.4 mm over the year, respectively [23,24]. The soils are Andic type, ferrallitic, trachytic, granitic, and basaltic [22,24,25].

This area is underlain by an extensive and thick loose mantle developed on trachyte and generally forms a differentiated geological profile, including the presence of deposits formed by new bauxite minerals; it was discovered in 1957 by BUMIFOM prospectors [26,27]. This locality is one of the main bauxite deposit sites in the western region of Cameroon. Its potential is estimated at 45 million tons and is a part of the major geological reserves of Cameroon [26,28]. Figure 1 shows a geological map of the study area.

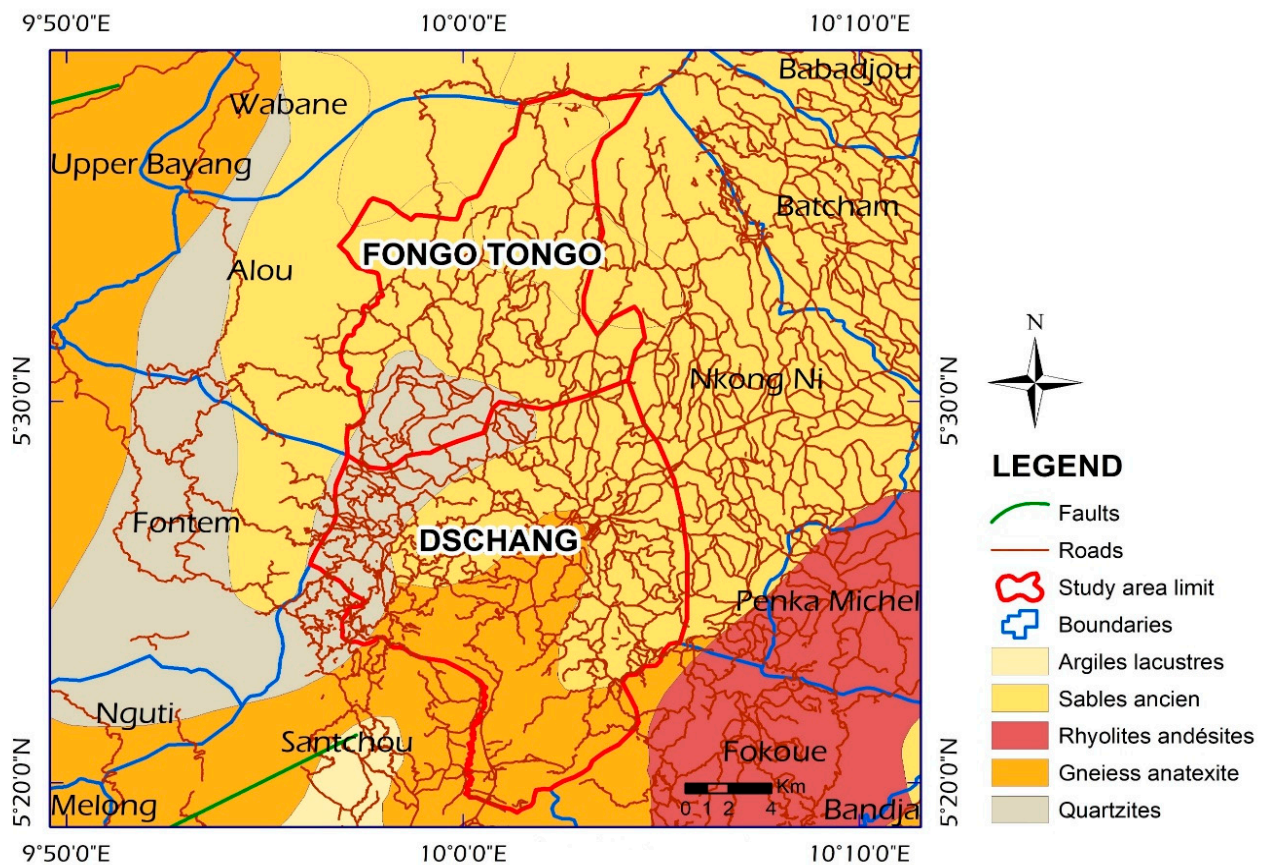


Figure 1. Soil characteristics map of the area.

2.2. Natural Radioactivity Measurements

2.2.1. Radioactivity Measurements in Laboratory

A total of twenty-seven soil samples (fifteen in Dschang and twelve in Fongo-Tongo) were randomly collected for a depth between 0 and 5 cm. The samples were collected, crushed, and then dried at 100 °C for 48 h to remove moisture and mold. Then they were crushed and filtered to a size of 1 mm, transferred to Marinelli containers of 500 cm³ each, tightly closed, and stored for at least 28 days to reach secular equilibrium between ²²²Rn and its decay products [29,30].

²²⁶Ra, ²³²Th, and ⁴⁰K activity concentrations were obtained by using a NaI (Tl) scintillation spectrometer Model 802 with a crystal size of 7.6 cm × 7.6 cm and a resolution of 7.5% at 661.6 keV, with a 1024-channels multichannel analyzer. It was calibrated in energy with reference sources containing ⁶⁰Co (1173.23 and 1332.5 keV), ¹³³Ba (383.9 keV), ⁵⁴Mn (834.9 keV), ²²Na (511 and 1274.5 keV), and ¹³⁷Cs (661.6 keV) from the IAEA and in efficiency by a multi-energy standard analyzed under the same experimental conditions as the samples [31,32]. This standard is a blend of different radioactive sources, forming an energy range from 59.54 to 1836 keV [⁶⁰Co (1173.2 and 1332.5 keV), ¹³⁷Cs (661.6 keV), ¹⁵²Eu (1407.5, 1112, 964.079, and 778.9 keV), ⁴⁰K (1460.8 keV), ¹³⁷Cs (661.6 keV), ²⁰⁸Tl (2614.4 keV), and ²²⁸Ac (940.1 keV)].

After reaching secular equilibrium between ²²²Rn and its progeny, a gamma-ray line at 609.3 KeV of ²¹⁴Pb was considered to determine the activity concentration of ²²⁶Ra, and a gamma-ray line at 969 KeV of ²²⁸Ac used to determine that of ²³²Th [33]. The spectra analysis was carried out by using GENIE 2000 (Canberra) software. ²²⁶Ra, ²³²Th, and ⁴⁰K activity concentrations in soil were determined by the following equation [17,34,35]:

$$A = \frac{N_p}{t_c \times I_\gamma(E_\gamma) \times \varepsilon(E_\gamma) \times M} \quad (1)$$

where N_p is the number of counts in a given peak area at energy, E ; $\varepsilon(E_\gamma)$ the detection efficiency at energy, E ; t_c is the counting time of 100,000 s; $I_\gamma(E_\gamma)$ is the number of gamma-rays per decay of that nuclide at energy, E , and M , the mass in kg, of the sample. The uncertainty on the activity concentration (ΔA) was obtained by the following equation [36,37]:

$$\frac{\Delta A}{A} = \sqrt{\left(\frac{\Delta N_p}{N_p}\right)^2 + \left(\frac{\Delta I_\gamma}{I_\gamma}\right)^2 + \left(\frac{\Delta \varepsilon}{\varepsilon}\right)^2 + \left(\frac{\Delta M}{M}\right)^2} \quad (2)$$

where ΔN , ΔI_γ , $\Delta \varepsilon$, and ΔM are the uncertainties in the count rate, emission probability found in the nuclear data tables, efficiency, and sample mass, respectively.

2.2.2. In Situ Radioactivity Measurements

They were performed simultaneously with sampling for laboratory analysis. Those measurements were made randomly at different points of the area with NucScout detector (portable Gamma Identifier-Quantifier—Dose Rate Meter) version 2018. It was installed one meter above the ground surface on a dry wooden stand. The measurement on a sample point took 45 min [38].

The NucScout is a high-sensitivity Na (Tl) gamma detector, with an integrated photo multiplier and high-voltage-supply cylindrical scintillation crystal, 2" × 2", with an energy range of 25 keV–3 MeV (optional from 10 keV to 1.6 MeV) and resolution < 8% (Cs-137/662 keV). It works with an integrated battery. The instrument has several options such as the selection of the measurement cycle, the reading, and the calculation of the results of a measurement. It has an integrated GPS that allows users to geolocate a sampling point, or even to bring out a Maps distribution of the different measured points. The data of the different measurements obtained on the site are stored on an a USB support or on an SD card and transferred for analysis and to a PC [39]. These data are visualized with the dvision software [40]. The detector is calibrated when connected to a PC, using the dconfig software [40]. ^{226}Ra , ^{232}Th , and ^{40}K activity concentrations were obtained by using gamma lines at 609.3 KeV of ^{214}Bi , 2614 KeV of ^{208}Tl , and 1461 of ^{40}K , respectively.

2.2.3. In Situ ^{222}Rn in Soil Measurements

Measurements were taken at different locations with Markus 10 version 1.4. This instrument was developed by RADONOVA Laboratories to measure the volumic activity of ^{222}Rn in soil, with about 3 kg and 16 keV of resolution energy (under vacuum); it is an ORTEC Ultra Silicon detector with dimensions of 220 × 122 × 80 cm³, with a pumping capacity of 1.8 L/min every 30 s, under a limiting pressure of 0.96 bar. The duration of a measurement is typically 12 min, and its battery has a capacity of about 70 measurements before being fully recharged for 8 h [41].

The principle of measurement of the device consists of two steps. The first step is the pumping phase of the gas contained in soil. This is achieved with a probe buried one meter in the ground. The gas is sucked from the ground into the measuring chamber for a short period. The pumping phase is automatically stopped when the pressure in the probe drops; when the pressure rises, the pump starts again. The pumping phase is finally stopped when a capacity of 0.91 L is reached. The next one is automatically started and consists of the measurement. The measuring chamber is immediately switched on. An electric field pushes the radon progeny into the measuring chamber, where the alpha radiation they emit is recorded. These electric pulses recorded by the sensor are amplified and then filtered in the analysis channel, which allows only the counting of pulses corresponding to the energy coming from the ^{218}Po . A latent measuring background is created in the ionization chamber of the system by filtering out the pulses from the ^{214}Po . The evolution of the measurement can be read on a screen, with each hit recorded by the sensor, until the screen displays a fixed value to signify the end of the measurement.

2.3. Radiological Hazards

2.3.1. Ambient Equivalent Dose Rates and External Effective Dose

Ambient equivalent dose rates in air at distance of one meter on the ground surface are calculated using the conversion factor of $0.0417 \text{ (nGy h}^{-1})/(\text{Bq kg}^{-1})^{-1}$ for ^{40}K , $0.462 \text{ (nGy h}^{-1})/(\text{Bq kg}^{-1})^{-1}$ for ^{226}Ra , and $0.604 \text{ (nGy h}^{-1})/(\text{Bq kg}^{-1})^{-1}$ for ^{232}Th in the following equation [1].

$$D(\text{nGy h}^{-1}) = 0.462A_{\text{Ra}} + 0.604A_{\text{Th}} + 0.0417A_{\text{K}} \quad (3)$$

where A_{Ra} , A_{Th} , and A_{K} are the mean concentrations of each radionuclide given in (Bq kg^{-1}) . The effective dose due to external irradiation, $E \text{ (mSv y}^{-1})$, was calculated by using the following formula [42,43]:

$$E(\text{mSv y}^{-1}) = F_{\text{c}}[F_{\text{occ}}F_{\text{b}} + (1 - F_{\text{occ}})] \times D \times T \times 10^{-6} \quad (4)$$

where $F_{\text{c}} = 0.7$ is the conversion coefficient of the absorbed dose in the air to effective dose received by adults, T is the exposure time expressed in hours, F_{b} (0.98) is the impact factor of the building material experimentally obtained on the site, and $F_{\text{occ}} = 0.8$ is the occupancy coefficient [1].

2.3.2. External and Internal Hazard Index

External Hazard Index (H_{ext})

The external hazard index was introduced to limit radiation exposure in the samples to a permissible dose-equivalent limit of 1.00 mSv y^{-1} [1,9,44], and it is assessed by Equation (5):

$$H_{\text{ext}} = \frac{A_{\text{Ra}}}{370} + \frac{A_{\text{Th}}}{259} + \frac{A_{\text{K}}}{4810} \leq 1 \quad (5)$$

The external hazard index must not exceed the limit of unity for the radiological risk to be insignificant. The maximum value of H_{ext} equal to unity corresponds to the upper limit of $370.00 \text{ Bq kg}^{-1}$ of ^{226}Ra [1,9,45].

Internal Hazard Index (H_{in})

Furthermore, the deposition period of ^{222}Rn progeny in the pulmonary is also very dangerous [5,44]. In order to take this threat into account and reach the normal limit of 185 Bq kg^{-1} , the permissible value for ^{226}Ra is reduced by half to reach the limit of the unit. It is evaluated by using the following equation [44,46]:

$$H_{\text{in}} = \frac{A_{\text{Ra}}}{185} + \frac{A_{\text{Th}}}{259} + \frac{A_{\text{K}}}{4810} \leq 1 \quad (6)$$

2.4. Excess Lifetime Cancer Risk (ELCR)

The ELCR is the probability that an individual will contract or develop a radiation-induced cancer during his lifetime because of his exposure to ionizing radiation. It was estimated for this by using Equation (7) [9,13,47]:

$$\text{ELCR} = \text{ELCR}_{\text{out}} + \text{ELCR}_{\text{in}} \quad (7)$$

$\text{ELCR}_{\text{out}} = E_{\text{out}} \times D_{\text{L}} \times \text{RF}$ is the outdoor risk; $\text{ELCR}_{\text{in}} = E_{\text{in}} D_{\text{L}} \times \text{RF}$ is the indoor risk; E_{out} and E_{in} are the indoor and outdoor effective dose, respectively; D_{L} is the average life expectancy of 70 years; and RF is the risk factor (risk of fatal cancer per mSv). In its publication 106, ICRP recommends value of $\text{RF} = 0.05 \times 10^{-3} \text{ mSv}^{-1}$ for induction to stochastic effects of members to the public [5].

2.5. Excess Cancer Risk (ECR) Computer Using RESRAD-ONSITE and RESRAD-BUILD Codes

Since most dwellings in the study are constructed with locally manufactured earthen or sand bricks, the ^{40}K , ^{226}Ra , and ^{232}Th concentrations in soil are input data (contaminant on source parameters) at runtime by RESRAD-ONSITE and RESRAD-BUILD codes version 7.2 and 3.5, respectively.

RESRAD-ONSITE is used to assess the ECR due to these naturally occurring radionuclides in soil at the bauxite-bearing area of Fongo-Tongo. The site-specific characteristics of the area are listed in Table 1. The other parameters are used as default values [48]. Together, all the above parameters were considered in the evaluation of the risk factors.

Table 1. Input parameters for RESRAD codes.

RESRAD-ONSITE	
Parameters	Site-Specific Data
Site-specific data	25,000 m ²
Cover depth	1 m
Density of contaminated zone	1.8 cm ³ g ⁻¹
Precipitation rate	0.4473 m y ⁻¹
Wind speed	1.2 m s ⁻¹
Well pump intake	8 m
RESRAD-BUILD	
Indoor/time fraction	0.6
Number of room/occupants	1
Deposition velocity	0.01 m s ⁻¹
Resuspension rate	5 × 10 ⁻⁷ s ⁻¹
Room surface area and volume	16 m ² and 40 m ³
Breathing rate	18 m ³ d ⁻¹
Ingestion rate	44,661
Occupant location in the room	Centered
Shielding thickness	0
Type of source	Volume
Source geometry	Rectangular
Release air fraction	0.1
Radon diffusion rate	2 × 10 ⁻⁵ m s ⁻¹
Porosity	0.1

RESRAD-BUILD allowed for the assessment of radiation doses received by a resident living or working in a house contaminated by radioactive materials. These doses are those from the different exposure pathways (external and internal, including inhalation of radon progeny inside the home). The radiological risk was estimated over the periods of 1, 10, 30, 50, 70, and 90 years of exposure. However, 85% of the dwellings in the area are made of mud bricks, usually produced on the same site, and samples of these earth bricks were analyzed to obtain the concentrations introduced as input data mentioned above. Table 1 presented the other input parameters.

2.6. Radiation Hazard Index

2.6.1. Gamma Radiation Hazard Index (I_γ)

The gamma radiation risk index was estimated from Equation (8) [47,49]:

$$I_\gamma = \frac{A_{\text{Ra}}}{300} + \frac{A_{\text{Th}}}{200} + \frac{A_{\text{K}}}{3000} \leq 1 \quad (8)$$

It is the index of nuclear energy level for external radiation due to specific activity of different natural radionuclides in a sample [50]. Its permissible limit is $I_\gamma = 1$ and corresponds to 0.3 mSv y⁻¹. It is used to evaluate the gamma-radiation risk level associated with naturally occurring radionuclides.

2.6.2. Alpha Radiation Hazard Index (I_α)

The excess alpha radiation following radon inhalation from building materials is determined by using Equation (9) [51,52]:

$$I_\alpha = \frac{A_{Ra}}{200} \leq 1 \quad (9)$$

The upper limit of I_α is unity because a building material with a ^{226}Ra concentration of less than 200 Bq kg^{-1} cannot cause a minimum radon concentration greater than 200 Bq m^{-3} .

3. Results and Discussion

3.1. ^{226}Ra , ^{232}Th , and ^{40}K Activity Concentrations

In Fongo-Tongo, the ^{226}Ra , ^{232}Th , and ^{40}K activity concentrations obtained by laboratory and in situ methods ranged from 106 to 170 Bq kg^{-1} and from 93 to 201 Bq kg^{-1} for ^{226}Ra ; from 119 to 295 Bq kg^{-1} and from 40 to 327 Bq kg^{-1} for ^{232}Th ; and from 188 to 458 Bq kg^{-1} and from 49 to 321 Bq kg^{-1} for ^{40}K .

In Dschang, the ^{226}Ra , ^{232}Th , and ^{40}K activity concentrations range from 99 to 167 Bq kg^{-1} and from 98 to 181 Bq kg^{-1} for ^{226}Ra , from 100 to 275 Bq kg^{-1} and from 139 to 309 Bq kg^{-1} for ^{232}Th ; and from 198 to 297 Bq kg^{-1} and from 151 to 280 Bq kg^{-1} for ^{40}K . Figure 2 shows the box-plot distributions of these concentrations in laboratory (a) and in situ (b) for each locality and for the whole study area.

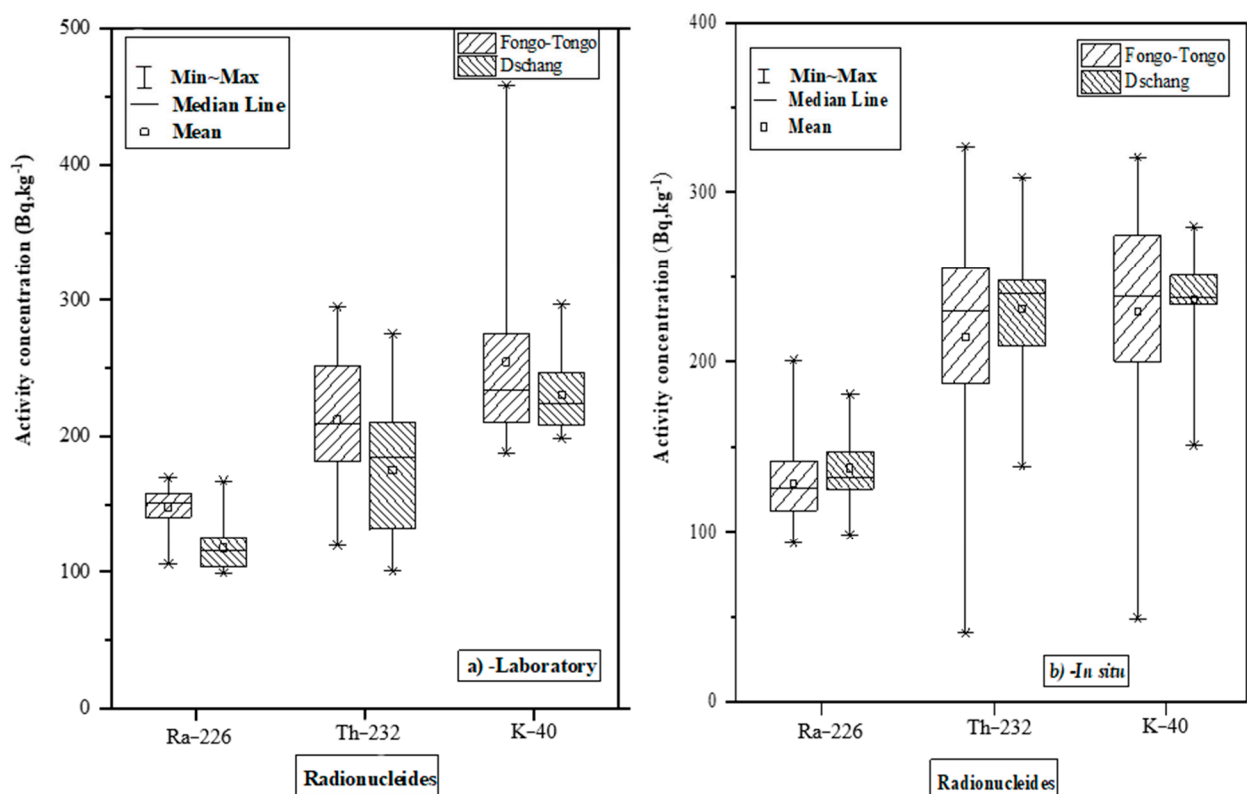


Figure 2. Boxplot distribution of activity concentration of ^{226}Ra , ^{232}Th , and ^{40}K obtained by laboratory (a) and in situ (b) measurements.

According to Table 2, 50% of sampling points have a concentration higher than 151 Bq kg^{-1} , 209 Bq kg^{-1} , and 234 Bq kg^{-1} for ^{226}Ra , ^{232}Th , and ^{40}K , respectively, in laboratory measurements. Furthermore, the in situ measurements follow a lognormal distribution. Thus, the mean value is represented by the geometric mean, whereas laboratory measurements follow a normal distribution and are represented by the arithmetic mean.

Table 2. Statistical parameters of ^{226}Ra , ^{232}Th , ^{40}K , and ^{222}Rn concentrations obtained by in situ and laboratory measurements for the localities of Dschang and Fongo-Tongo.

Locality	Parameters	Activity Concentration (Bq kg^{-1})					^{222}Rn (kBq m^{-3})	
		^{226}Ra	Laboratory ^{232}Th	^{40}K	^{226}Ra	In situ ^{232}Th		^{40}K
Fongo-Tongo	Min–Max	106–170	119–295	188–458	93–201	94–327	49–321	35–202
	Median	151	209	234	126	229	239	53
	AM \pm SD	148 ± 23	212 ± 54	230 ± 28	-	-	-	-
	GM(GSD)	-	-	-	129 (16)	214 (67)	229 (54)	69 (8)
Dschang	Min–Max	99–167	100–275	198–297	98–181	139–309	151–280	48–255
	Median	116	185	224	132	240	238	62
	AM \pm SD	118 ± 17	175 ± 46	230 ± 28	-	-	-	-
	GM(GSD)	-	-	-	138 (19)	231 (35)	237 (26)	82 (14)

AM, arithmetic mean; GM, geometric mean; SD, standard deviation; GSD, geometric standard deviation.

Soil samples analyzed in the laboratory have high concentrations of ^{226}Ra and ^{232}Th . As presented in Table 2, the minimum and maximum values of ^{226}Ra obtained in laboratory and in situ measurements are, respectively, three and five times higher than the world average value of 35 Bq kg^{-1} [1]. In the case of ^{232}Th , they are two and four times higher than the world average value of 45 Bq kg^{-1} , respectively [1]. These high values of ^{226}Ra and ^{232}Th activity concentrations are also observed for the results obtained by in situ gamma spectrometry. The minimum values of ^{226}Ra and ^{232}Th are, respectively, three and two times higher than the world average value, while the maximum values are, respectively, six and seven times higher than the world average value [1]. Furthermore, the average values of ^{40}K , as well as the maximum values for in situ and laboratory methods, are lower than 420 Bq kg^{-1} , the world average value [1].

Figure 1 shows that the investigated area extends over a geological structure covered by basaltic and trachytic granitic rocks [27,53]. The ^{226}Ra , ^{232}Th , and ^{40}K activity concentrations differ from one point to another for the two techniques used: in situ and laboratory gamma spectrometry. This can be explained by the fact that radioactivity is not uniformly distributed in the soil [54]. It is reported that ^{238}U , ^{232}Th , and ^{40}K have high concentrations in some rocks, such as syenite, granite, granulite, rhyolites, and plutonic [3,4,54]. The low concentrations of ^{40}K can be explained by the phenomenon of leaching and transport of potassium elements to the surface due to the effects of erosion, drainage, and an accumulation of sediments in the seabed [55]. The transfer of ores by erosion or by eruptive voice can therefore considerably modify the content and concentrations of this radionuclide in the soil. It has low concentrations in basalt [3,4,54]. According to Figure 1, the presence of the above rocks can account for considerable variation in the concentrations of these primordial radionuclides from one site to another, as shown in Figure 2.

3.2. In Situ ^{222}Rn Concentration in Soil

^{222}Rn concentrations at 1 m depth in soil, presented in Table 2, ranged from 35 to 202 kBq m^{-3} , with a mean value of $69 \pm 40 \text{ kBq m}^{-3}$, in Fongo-Tongo; and from 48 to 255 kBq m^{-3} , with a mean value of $82 \pm 56 \text{ kBq m}^{-3}$, in Dschang. According to Table 2, more than half of the sampled points have ^{222}Rn in soil greater than or equal to 62 kBq m^{-3} in Dschang and 53 kBq m^{-3} in Fongo-Tongo. According to Figure 3, a majority of the radon concentrations in soil are above the value of 40 kBq m^{-3} , as represented by the red line. According to the Swedish risk assessment criteria, this latter value represents the limit for which a site presents a high radon-exposure risk [56]. The difference between ^{222}Rn concentrations in soil from one location to another may be due to the geological structure and the mineralogical composition of the soil in the area [54,55]. The geological structure, the geochemical process of the soil, and the rate of gas emanation in the region are influenced by the permeability of the soil [27,28,49,53,54].

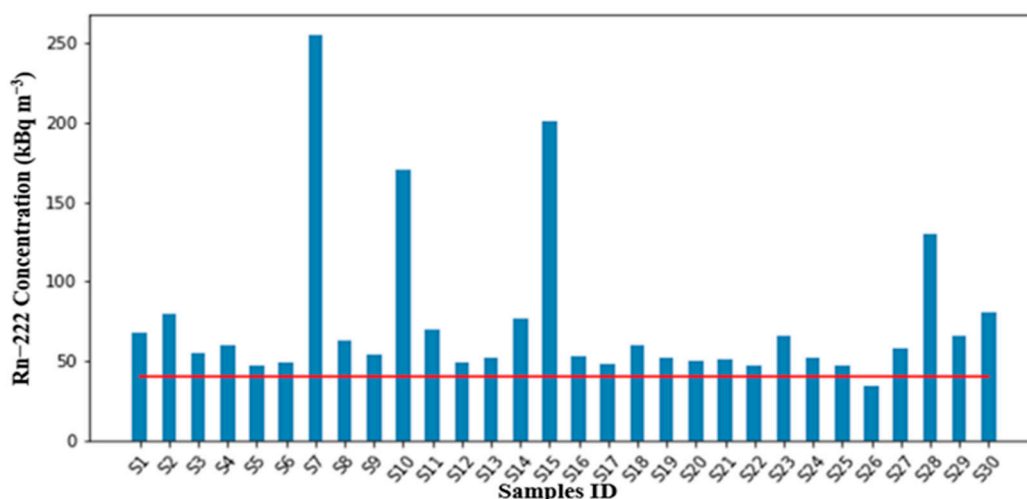


Figure 3. ²²²Rn distribution in soil of the bauxite bearing area of Fongo-Tongo.

Table 2 shows that the average and maximum values of ²²²Rn in soil in Dschang are higher than those in Fongo-Tongo. This is not the case with the ²²⁶Ra values obtained in these two localities. This is probably due to the influence of soil moisture and porosity. In addition, the soil in the Fongo-Tongo may be more compact and moister than in Dschang [25,53]. In additional, Table 3 shows that activity concentrations of the primordial radionuclides in soil in Cameroon is higher than in some other regions of the world [51,52,57,58]. Nevertheless, ⁴⁰K concentrations are also high elsewhere than in the present study [46,52].

Table 3. Comparison of ²²⁶Ra, ²³²Th, ⁴⁰K, and ²²²Rn activity concentration with other countries.

Country	Activity Concentration (Bq kg ⁻¹)			²²² Rn (kBq m ⁻³)	References
	²²⁶ Ra	²³² Th	⁴⁰ K		
Jordan	57.7 ± 5.4	18.1 ± 1.4	138.1 ± 40.8		[46]
Egypt	134.7 ± 24.1	131.8 ± 16.7	11,644 ± 550		[59]
India	116.1	43.51	300.07	-	[37]
Iraq	58.44	19.38	321.76	-	[9]
	45.71	20.33	337.02	-	
Nigeria	64.64 ± 28.10	110.18 ± 46.12	1190.10 ± 373.62		[51]
Australia	38	45	635	-	[10]
Germany	84	72	463	-	
Sweden	75	94	734	-	
Japan	38 ± 1	43 ± 1	590	-	[8]
Cameroon	14 ± 2	30 ± 3	103 ± 12	9 ± 2	[60]
	-	390	850	-	[14]
	124.9	157.3	670.9		[61]
	166.18	170.04	94.54		[13]
	118 ± 17 (138 ± 19)	175 ± 46 (231 ± 35)	230 ± 28 (237 ± 26)	82 ± 56	Present study
	148 ± 23 (129 ± 16)	212 ± 54 (214 ± 67)	230 ± 28 (229 ± 54)	69 ± 40	

3.3. Correlation between ²²²Rn and ²²⁶Ra in Soil

According to Figure 4, it is shown that ²²²Rn concentrations in soil are directly related to those of ²²⁶Ra measured at the site and in soil samples collected in the area. The R² = 0.88 and R² = 0.86 values were found between ²²²Rn and ²²⁶Ra concentrations for the laboratory method and in situ method, respectively. These high values of the coefficients obtained for each case reveal that ²²²Rn and ²²⁶Ra are strongly correlated. Similarly, the Pearson correlation coefficient determined for both sets of measurements is equal to 0.92 for the

laboratory and 0.90 for in situ. These respective Pearson correlation coefficients for the two series confirm the strong correlation between the two radionuclides.

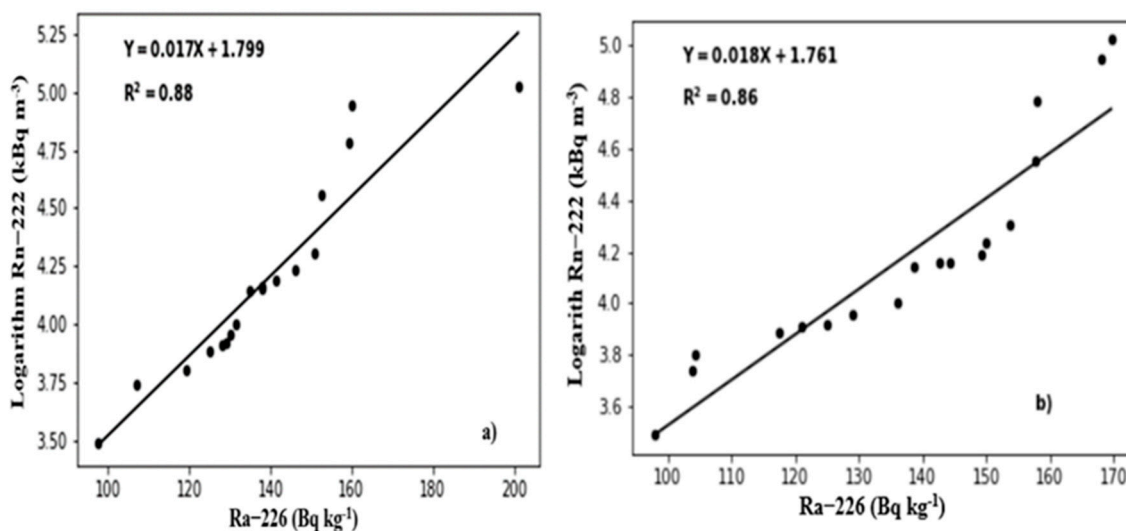


Figure 4. Correlation between $^{222}\text{Rn}/^{226}\text{Ra}$ concentrations in soil: (a) laboratory gamma-ray spectrometry and (b) in situ gamma-ray spectrometry.

For the values observed between 110 and 150 Bq kg^{-1} (Figure 4a) and values between 130 and 160 Bq kg^{-1} (Figure 4b), the residual is relatively constant, and for the extreme values, it increases slightly, which shows a dispersion of the maximum values from the median value. This can be justified by the fact that the number of samples of the different datasets is not very high to make the scatterplot dense enough and have a better regression. That is, the closer in the series values are to each other, the better correlation the coefficient and the stronger correlation intensity. This also means that, the smaller the standard deviation is between the data, the better the regression and the stronger the correlation between the two radionuclides.

The high values of ^{222}Rn concentration in soil gas at some locations certainly originate from the deep sources of permeable soil, which allows ^{222}Rn to easily escape from its cradle, which is ^{226}Ra , and migrate to the free surface of the soil. In other words, the high emanation of ^{222}Rn at a measurement point is closely related to the nature of underlying rock, geochemical process, physicochemical soil properties, and ^{226}Ra content in soil. The correlation observed between these concentrations depends on the geological structure of the area [62]. Similar results are reported in previous studies [47,63].

As shown in Figure 1, the area contains different rock formations, such as granite, basalt, gneiss, and trachyte. In addition, it is characterized by a deposit of bauxite ores [26,27]. Granite, mined in quarries in Dschang and Fongo-Tongo, is probably a potential source of ^{226}Ra distributed in the area. It is known to have a high content of uranium, thorium, and potassium at high temperatures in these rocks [54]. ^{222}Rn emanation may therefore be stronger in an area underlain by granitic bedrock.

Figure 5 shows the distribution map of ^{222}Rn and ^{226}Ra activity concentrations in the soil of the study area. It shows that the activity concentration of ^{226}Ra in soil increases with the ^{222}Rn concentration in its close proximity.

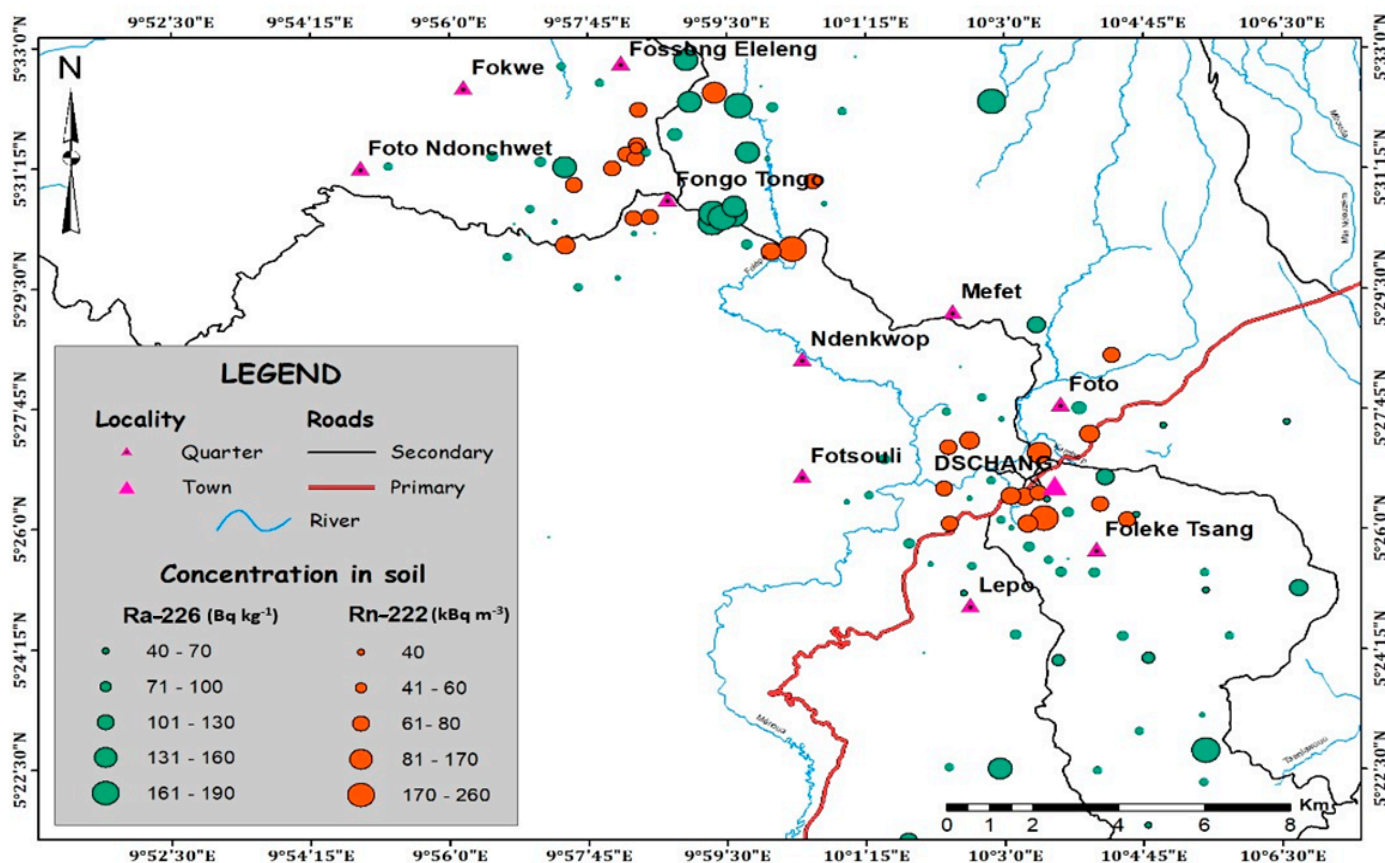


Figure 5. Map distribution of ²²²Rn and ²²⁶Ra concentrations in the soil of the study area.

3.4. Radiological Hazards

3.4.1. Ambien Equivalent Dose Rate (AEDR) and Annual External Effective Dose (AEED)

The AEED obtained in the laboratory ranged from 0.58 to 1.62 mSv y⁻¹, with a mean value of 1.27 ± 0.27 mSv y⁻¹, in Fongo-Tongo; and from 0.73 to 1.46 mSv y⁻¹, with a mean value of 1.05 ± 0.17 mSv y⁻¹, in the Dschang locality. According to Table 4 the average values for the whole study area are above the safety limit of 1.00 mSv y⁻¹ [1].

Table 4. Summary of the different radiological parameters obtained in laboratory.

Locality Parameters	Fongo-Tongo					Dschang					Limit
	Min	Max	Med	AM	SD	Min	Max	Med	AM	SD	
AEDR (nGy/y)	130	265	211	207	37	119	238	172	170	31	1
AEED (mSv)	0.8	1.62	1.29	1.27	0.22	0.73	1.46	1.05	1.04	0.19	1
H _{in}	1.36	2.81	1.82	1.88	0.37	1.36	1.92	1.57	1.6	0.15	1
H _{out}	1.07	2.35	1.41	1.48	0.33	1.29	1.58	1.29	1.29	1.02	1
ELCR _{in}	1.68	3.4	2.71	2.67	0.47	1.53	3.06	2.21	2.18	0.4	
ELCR _{out}	1.12	2.26	1.81	1.78	0.31	1.02	2.04	1.47	1.46	0.27	
ELCR	2.59	5.66	4.52	4.44	0.78	2.55	5.11	3.69	3.64	0.66	
I _α	0.53	0.85	0.76	0.74	0.08	0.49	0.84	0.58	0.59	0.09	1
I _γ	1.02	2.11	1.66	1.64	0.3	0.93	1.9	1.36	1.34	0.25	1

AM, arithmetic mean; GM, geometric mean; SD, standard deviation; GSD, geometric standard deviation.

According to Table 5, the AEDR at one meter above ground surface ranged from 130 to 265 nGy h⁻¹ and from 119 to 238 nGy h⁻¹ at Fongo-Tongo and Dschang, respectively, with an average of 207 ± 37 nGy h⁻¹ and 170 ± 31 nGy h⁻¹ for soil samples analyzed in the laboratory. It ranged from 95 to 264 nGy h⁻¹ and from 69 to 126 nGy h⁻¹, with a mean value of 198 ± 45 nGy h⁻¹ and 96 ± 14 nGy h⁻¹, for the in situ measurement in

Fongo-Tongo and Dschang, respectively. The mean values of the current studies are all above the value set of 60 nGy h^{-1} [1].

Table 5. Summary of the different radiological parameters obtained by in situ.

Locality Parameters	Fongo-Tongo					Dschang					Limit
	Min	Max	Med	AM	SD	Min	Max	Med	AM	SD	
AEDR (nGy/y)	95	264	210	198	45	69	126	94	96	14	1
AEED (mSv)	0.58	1.62	1.27	1.22	0.28	0.42	0.77	0.58	0.59	0.08	1
H_{in}	0.9	2.01	1.65	1.57	0.32	1.25	2.04	1.68	1.68	0.19	1
H_{out}	0.56	1.64	1.3	1.22	0.29	0.92	1.64	1.32	1.31	0.16	1
ELCR _{in}	1.22	3.4	2.71	2.56	0.58	0.89	1.62	1.21	1.24	0.17	
ELCR _{out}	0.81	2.7	1.8	1.7	0.31	0.59	1.08	0.81	0.83	0.11	
ELCR	2.03	5.67	4.51	4.26	0.97	1.48	2.7	2.01	2.07	0.28	
I_{α}	0.47	1.01	0.63	0.64	0.11	0.49	0.9	0.66	0.69	0.09	1
I_{γ}	0.72	2.12	1.67	1.58	0.37	1.19	2.12	1.7	1.69	0.21	1

AM, arithmetic mean; GM, geometric mean; SD, standard deviation; GSD, geometric standard deviation.

3.4.2. External and Internal Radiation Hazard Index

External Hazard Index

The obtained values of H_{ext} are presented in Table 4. The average values are 1.48 at Fongo-Tongo and 1.32 at Dschang. H_{ext} values are greater than unity, and therefore, it can be recommended to the populations of those sites to use earth as a building construction material, except in some places where the level of natural radioactivity is relatively high.

Internal Hazard Index

The statistical parameters from H_{in} are summarized in Table 4. The maximum values of H_{in} are 2.81 and 2.04, with an average value of 1.88 and 1.68, in Fongo-Tongo and Dschang, respectively. H_{in} values are also greater than unity [64]. Nevertheless, to avoid excessive internal exposure to ^{222}Rn in these localities, the use of earth can be recommended as a building material, provided that there is good ventilation and air circulation in the rooms of the dwelling.

3.4.3. Excess Lifetime Cancer Risk (ELCR)

The ELCR statistical parameters' values obtained by gamma spectrometry in laboratory and in situ are summarized in Table 4. They ranged from 2.03×10^{-3} to 5.67×10^{-3} , with a mean value of 4.44×10^{-3} , in Fongo-Tongo; and from 1.48×10^{-3} to 5×10^{-3} , with a mean value of 3.64×10^{-3} , in Dschang. The mean values of ECR in Fongo-Tongo and Dschang were, respectively, 1.29 and 1.06 times higher than 0.29×10^{-3} , the UNSCEAR recommended limit value [1]. However, the risk values obtained could be overestimated if, in addition to the above risk, the risk due to radioactivity from building materials was taken into account, because more than 70% of the houses in the area use mainly mud bricks as building material.

3.5. Long-Term ECR Analysis Using RESRAD-ONSITE and RESRAD-BUILD Computer Codes

As shown in Figure 6, the total ECR calculated with RESRAD-ONSITE decreased progressively over the years, from the maximum value of 8.58×10^{-3} obtained at the dates $T = 1$ and $T = 1$ year to the value of 7.41×10^{-3} obtained at $T = 100$ years before decreasing significantly. This remarkable decreasing may be due to the self-absorption of building materials or to the process of radioactive decay [65].

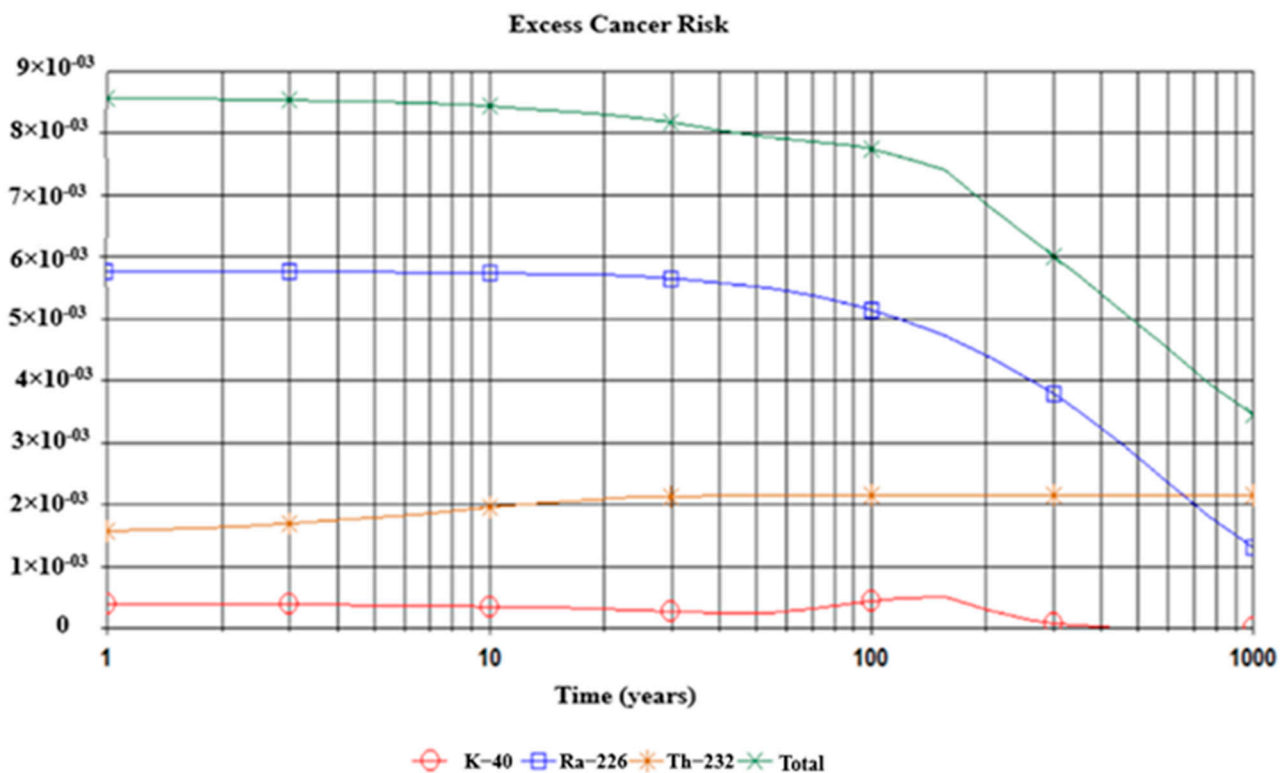


Figure 6. Long-term plotting of ECR for all exposure pathways and for each primordial radionuclide.

Similarly, ^{226}Ra is the major contributor to the total ECR at about 70% in the first year. This contribution decreases slightly over the years before dropping significantly after 100 years. The maximum value of risk due to ^{226}Ra obtained at $T = 10$ years is 7.372×10^{-6} . The ECR due to ^{232}Th , on the other hand, is inversely proportional to that of ^{226}Ra over the period from 1 to 40 years, where it becomes practically constant, and the maximum value obtained at $T = 50$ years is 9.250×10^{-6} . As for ^{40}K , its contribution to the total risk remains the smallest, but it shows some slight variations before decreasing to zero. Similar results were observed in studies conducted in the cobalt–nickel region of Lomié in Eastern Cameroon [66]. Table 5 summarizes the total ECR for initially existent radionuclides and pathways at $T = 0, 1, 10, 30, 50,$ and 100 years.

RESRAD-BUILD assessed the total risk due to radioactivity from soil used in the manufacture of bricks as a building material. The results obtained for the different exposure routes and for each nuclide as a function of time are summarized in Table 2. The maximum value of the total excess risk obtained at $T = 30$ years is 5.19×10^{-2} for all the summed routes. Similarly, the value of the total excess risk for all summed nuclides obtained at $T = 30$ years is 1.89×10^{-2} . However, it should be noted that the external pathway is the one that contributes the most to the total excess risk. The maximum risk value for this pathway, which is 2.33×10^{-2} , was obtained at $T = 30$ years. Nevertheless, the decrease observed beyond 30 years for the external route would be due to the self-absorption of building materials [15,67,68]. Similar results were obtained in the work carried out in the Poli uranium region [17], in the bauxite zones of Southern Adamawa [16], and in some localities of the Centre Region, Cameroon [67].

The results presented in Table 6 show that ^{226}Ra is the main contributor to the total excess risk compared to ^{232}Th and ^{40}K . The risk due to ^{226}Ra increases progressively with time until reaching an increasing threshold after 70 years. The occurrence of this radionuclide in high concentrations in building materials increases the probability of accumulation of high indoor radon concentration [68]. Figure 7 represents the long-term total ECR for each radionuclide.

Table 6. Total ECR for initially existent radionuclides and pathways and fraction of total risk.

T (Years)	Ground	Inhalation	Radon	Plant	Meat	Milk	Soil	Total
0	1.74×10^{-3}	6.32×10^{-6}	4.89×10^{-3}	1.56×10^{-3}	2.24×10^{-4}	1.44×10^{-4}	2.22×10^{-5}	8.58×10^{-3}
1	1.74×10^{-3}	6.32×10^{-6}	4.89×10^{-3}	1.56×10^{-3}	2.24×10^{-4}	1.44×10^{-4}	2.22×10^{-5}	8.58×10^{-3}
3	1.73×10^{-3}	6.32×10^{-6}	4.87×10^{-3}	1.55×10^{-3}	2.18×10^{-4}	1.42×10^{-4}	2.22×10^{-5}	8.54×10^{-3}
10	1.72×10^{-3}	6.30×10^{-6}	4.81×10^{-3}	1.53×10^{-3}	2.06×10^{-4}	1.36×10^{-4}	2.20×10^{-5}	8.43×10^{-3}
30	1.69×10^{-3}	6.27×10^{-6}	4.67×10^{-3}	1.49×10^{-3}	1.76×10^{-4}	1.24×10^{-4}	2.17×10^{-5}	8.17×10^{-3}
100	1.60×10^{-3}	6.18×10^{-6}	4.19×10^{-3}	1.38×10^{-3}	1.16×10^{-4}	9.75×10^{-5}	2.04×10^{-5}	7.41×10^{-3}

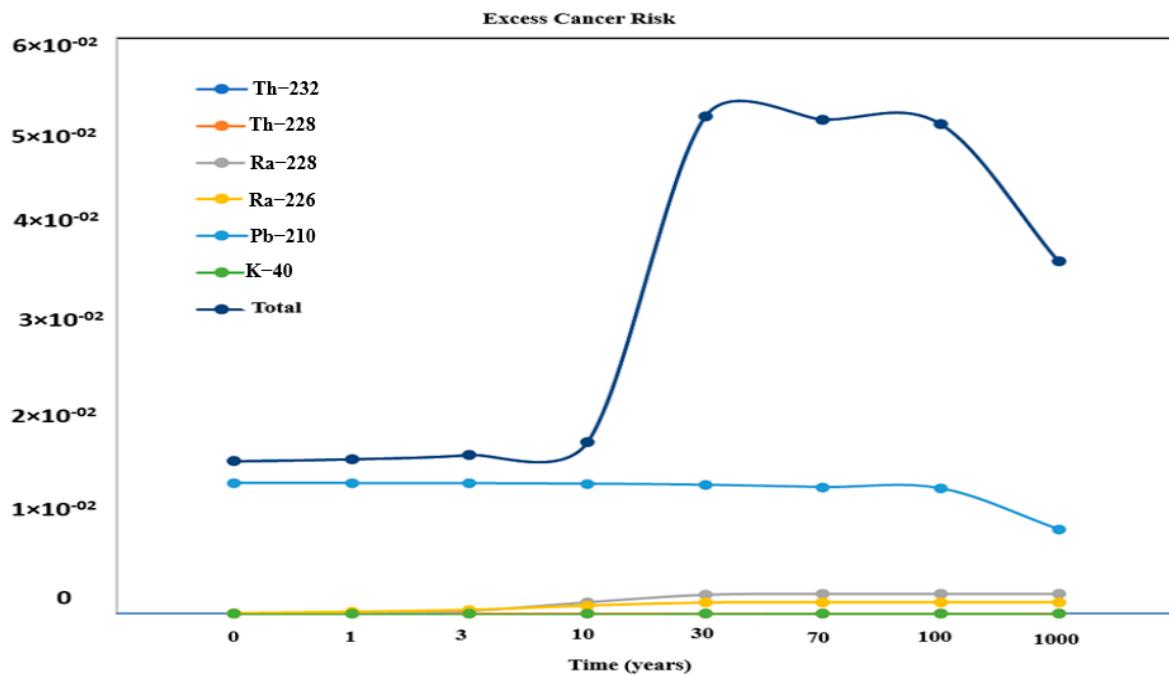


Figure 7. Long-term total excess risk for each nuclide.

According to Table 7, the pathway that contributes most to the total cancer risk is the external pathway. Like the other pathways, the risk increases until it reaches a value of 2.33×10^{-2} at T = 30 years. Similarly, the total cancer risk also increases and reaches a value of 5.19×10^{-2} at the same date.

Table 7. Total risk of excess cancer for all exposure pathways.

Pathway Detail of Risks	ELCR						
	T = 0	T = 1	T = 3	T (Years) T = 10	T = 30	T = 70	T = 100
External	1.57×10^{-2}	1.59×10^{-2}	1.63×10^{-2}	1.76×10^{-2}	2.33×10^{-2}	2.32×10^{-2}	2.30×10^{-2}
Deposition	5.15×10^{-9}	5.22×10^{-9}	5.31×10^{-9}	5.64×10^{-9}	3.68×10^{-3}	3.66×10^{-3}	3.63×10^{-3}
Immersion	4.50×10^{-11}	4.54×10^{-11}	4.65×10^{-11}	5.06×10^{-10}	3.68×10^{-3}	3.66×10^{-3}	3.63×10^{-3}
Inhalation	1.18×10^{-6}	1.23×10^{-6}	1.36×10^{-6}	1.76×10^{-6}	3.01×10^{-3}	2.99×10^{-3}	2.96×10^{-3}
Radon	2.20×10^{-4}	2.27×10^{-4}	2.49×10^{-4}	3.30×10^{-4}	4.08×10^{-3}	4.06×10^{-3}	4.03×10^{-3}
Ingestion	5.39×10^{-8}	5.88×10^{-8}	6.82×10^{-8}	8.39×10^{-8}	1.89×10^{-2}	1.88×10^{-2}	1.86×10^{-2}
Total	1.59×10^{-2}	1.61×10^{-2}	1.66×10^{-2}	1.79×10^{-2}	5.19×10^{-2}	5.15×10^{-2}	5.11×10^{-2}

3.6. Radiation Hazard Index

3.6.1. Gamma Radiation Hazard Index, I_γ

The results obtained give maximum values of I_γ equal to 2.12 and 2.67 at Fongo-Tongo and equal to 2.12 and 1.90 at Dschang for in situ and laboratory measurements, respectively,

which are significantly greater than or equal to 2 to 2.7 times the maximum permissible value [50]. Similarly, the mean values of 1.69 and 1.34 at Dschang and 1.58 and 1.64 at Fongo-Tongo are also above the recommended limit. Thus, the land in the region could be exempted from all types of restrictions with respect to radiological risks, except at certain locations where I_γ is very high.

3.6.2. Alpha Radiation Hazard Index, I_α

The average values of I_α are reported in Table 4 and are below the reference limit value of unity for both study sites. Therefore, the soil bricks made at the study sites can be used as a building material in these two localities without exposing the inhabitant to a major risk of induction of lung cancer, because the I_α is below the safety limit recommended by UNSCEAR.

4. Conclusions

The current work was performed to study the ^{222}Rn and ^{226}Ra correlation that may exist in soil and assess the onsite and in-dwellings long-term ECR in the bauxite-bearing area of Fongo-Tongo. To achieve this, gamma spectrometry by in situ and laboratory was used to determine activity concentrations of ^{226}Ra in soil. A strong correlation was found between ^{226}Ra determined from the two methods and ^{222}Rn in the soil. The ^{222}Rn measurement in soil is therefore an excellent predictor of ^{226}Ra and vice versa. Radiological parameters such as AEED, H_{in} , H_{ext} , ELCR, I_γ , and I_α were also determined to assess the level of radiological exposure of the public. Their values were all higher than the various corresponding safety limits recommended by UNSCEAR. The cancer risk assessed with RESRAD-ONSITE following exposure to the various radionuclides decreases from the first to the hundredth year for all the primordial radionuclides. The risk tends toward zero after the thousandth year. The maximum value of the total cancer risk of 8.58×10^{-3} was observed at $t = 1$ year. It should also be noted that the contribution of ^{226}Ra to cancer risk is high compared to that of ^{232}Th . ^{226}Ra is therefore the major contributor to cancer risk. A decrease in the contribution of all exposure pathways is observed from $t = 1$ year to $t = 100$ years. The risk tends to decrease considerably after 100 years. The cancer risk due to inhalation of radon and its progeny increases and reaches a peak of 3.01×10^{-3} at $t = 70$ years. It should be noted that RESRAD-BUILD evaluates the risk related to radon and thoron according to the concentration of radium and thorium. Given the high concentrations of ^{232}Th in soil samples from the current study area, the contribution of thoron (^{220}Rn) to cancer risk is high. Nevertheless, the observed decrease over time for all pathways and all radionuclides could be due to the self-absorption of building materials.

Author Contributions: Conceptualization, L.B.D. and S.; methodology, L.B.D., G.S.B. and S.; software, L.B.D., O.B.M. and J.E.N.N.II validation, L.B.D., G.S.B., and S.; formal analysis, L.B.D., J.E.N.N.II and S.; writing—original draft preparation, L.B.D., O.B.M. and G.S.B.; funding acquisition, S. All authors have read and agreed to the published version of the manuscript.

Funding: This work was partly supported by the International Atomic Energy Agency (IAEA) within the framework of the Technical Cooperation (TC) Project CMR9009. The Government of Cameroon supported field works through the Public Investment Budget 2020 and 2021 of the Ministry of Scientific Research and Innovation.

Institutional Review Board Statement: Not applicable.

Informed Consent Statement: Not applicable.

Data Availability Statement: The authors confirm that the data supporting the findings of this study are available within the article.

Acknowledgments: The Ministry of Scientific Research and Innovation of Cameroon is acknowledged for funding the field works through the Public Investment Budget 2021 allocated to the Institute of Geological and Mining Research.

Conflicts of Interest: The authors declare no conflict of interest.

References

1. UNSCEAR. *Sources and Effects of Ionizing Radiation: United Nations Scientific Committee on the Effects of Atomic Radiation: UNSCEAR 2000 Report to the General Assembly, with Scientific Annexes*; United Nations: Vienna, Austria, 2000.
2. Barbarand, J.; Beaufort, D.; Benedicto, A.; Caillat, C.; Calas, G.; Cathelineau, M.; Cheilletz, A.; Cote, G.; Cuney, M.; Dacheux, N.; et al. Géologie et Chimie de l'Uranium Programme et volume des résumés. In Proceedings of the Réunion de la Société Géologique de France avec le concours d'AREVA, CNRS—INSU, PACEN, GUTEC, IDES, Université de Paris-Sud, Paris, France, 29–30 November 2011.
3. Holmes, A. Petrogenesis of katungite and its associates. *Am. Mineral.* **1950**, *35*, 772–792.
4. Bariand, J.G.P.; Cesbron, F. Métamorphiques et leurs produits d'altération, par P. Bariand, F. *Bull. Minér. Cristallogr.* **1978**, *2*, 356.
5. Paquet, F.; Bailey, M.; Leggett, R.; Lipsztein, J.; Marsh, J.; Fell, T.; Smith, T.; Nosske, D.; Eckerman, K.; Berkovski, V.; et al. ICRP Publication 137: Occupational Intakes of Radionuclides: Part 3. *Ann. ICRP* **2017**, *46*, 1–486. [[CrossRef](#)]
6. Clement, C.; Tirmarche, M.; Harrison, J.; Laurier, D.; Paquet, F.; Blanchardon, E.; Marsh, J. Part 1: Lung Cancer Risk from Radon and Progeny. *Ann. ICRP* **2010**, *40*, 11. [[CrossRef](#)] [[PubMed](#)]
7. Lindsay, R.; Newman, R.; Speelman, W. A study of airborne radon levels in Paarl houses (South Africa) and associated source terms, using electret ion chambers and gamma-ray spectrometry. *Appl. Radiat. Isot.* **2008**, *66*, 1611–1614. [[CrossRef](#)] [[PubMed](#)]
8. Hassan, N.M.; Ishikawa, T.; Hosoda, M.; Sorimachi, A.; Tokonami, S.; Fukushima, M.; Sahoo, S.K. Assessment of the natural radioactivity using two techniques for the measurement of radionuclide concentration in building materials used in Japan. *J. Radioanal. Nucl. Chem. Artic.* **2010**, *283*, 15–21. [[CrossRef](#)]
9. Mohammed, R.S.; Ahmed, R.S. Estimation of excess lifetime cancer risk and radiation hazard indices in southern Iraq. *Environ. Earth Sci.* **2017**, *76*, 303. [[CrossRef](#)]
10. Trevisi, R.; Leonardi, F.; Risica, S.; Nuccetelli, C. Updated database on natural radioactivity in building materials in Europe. *J. Environ. Radioact.* **2018**, *187*, 90–105. [[CrossRef](#)]
11. Abiama, P.E.; Tokonami, S.; Patrice, E.A. Natural Radiation Survey in the Uranium and Thorium Bearing Regions of Cameroon. 2016. Available online: https://www.researchgate.net/publication/293593746_Natural_radiation_survey_in_the_uranium_and_thorium_bearing_regions_of_Cameroon (accessed on 5 September 2022).
12. Didier, T.S.S.; Saïdou, Tokonami, S.; Hosoda, M.; Suzuki, T.; Kudo, H.; Bouba, O. Simultaneous measurements of indoor radon and thoron and inhalation dose assessment in Douala City. *Cameroon. Isot. Environ. Health Stud.* **2019**, *55*, 499–510. [[CrossRef](#)]
13. Yimele, B.C.; Ekobena, H.P.F.; Nguelem, E.J.M.; Ndontchueng, M.M.; Ben-Bolie, G.H.; Ateba, P.O. Radiation hazard of naturally occurring soil in FONGO TONGO-Cameroon. *Arab. J. Geosci.* **2019**, *12*, 233. [[CrossRef](#)]
14. Mekongtso Nguelem, E.J.M.; Ndontchueng, M.M.; Motapon, O. Determination of ^{226}Ra , ^{232}Th , ^{40}K , ^{235}U and ^{238}U activity concentration and public dose assessment in soil samples from bauxite core deposits in Western Cameroon. *SpringerPlus* **2016**, *5*, 1253. [[CrossRef](#)] [[PubMed](#)]
15. Bachirou, S.; Joseph, I.I.; Ndjana, E.; Haman, F.; Godfroy, M.; Njock, K. Natural Radiation Exposure and Radiological Hazard Analysis in a Radon-Prone Area of the Adamawa Region, Cameroon. *Radiat. Prot. Dosim.* **2022**, *198*, 74–85.
16. Saïdou; Modibo, O.B.; Emmanuel, N.N.I.J.; German, O.; Michaux, K.N.; Abba, H.Y. Indoor Radon Measurements Using Radon Track Detectors and Electret Ionization Chambers in the Bauxite-Bearing Areas of Southern Adamawa, Cameroon. *Int. J. Environ. Res. Public Health* **2020**, *17*, 6776. [[CrossRef](#)] [[PubMed](#)]
17. Saïdou; Shinji, T.; Hosoda, M.; Flore, T.S.Y.; Emmanuel, N.N.I.J.; Naofumi, A.; Modibo, O.B.; Joseph, P. Natural radiation exposure to the public in the uranium bearing region of Poli, Cameroon: From radioactivity measurements to external and inhalation dose assessment. *J. Geochem. Explor.* **2019**, *205*, 106350. [[CrossRef](#)]
18. Ndjana Nkoulou, J.E.; Ngoa Engola, L.; Hosoda, M.; Bongue, D.; Suzuki, T.; Kudo, H.; Kwato Njock, M.G.; Tokonami, S. Simultaneous indoor radon, thoron and thoron progeny measurements in betare-oya gold mining areas, eastern Cameroon. *Radiat. Prot. Dosim.* **2019**, *185*, 391–401. [[CrossRef](#)]
19. Bineng, G.S.; Saïdou; Tokonami, S.; Hosoda, M.; Siaka, Y.F.T.; Issa, H.; Suzuki, T.; Kudo, H.; Bouba, O. The Importance of Direct Progeny Measurements for Correct Estimation of Effective Dose Due to Radon and Thoron. *Front. Public Health* **2020**, *8*, 17. [[CrossRef](#)]
20. Saïdou; Tokonami, S.; Janik, M.; Samuel, B.G.; Abdourahimi; Emmanuel, N.N.I.J. Radon-thoron discriminative measurements in the high natural radiation areas of southwestern Cameroon. *J. Environ. Radioact.* **2015**, *150*, 242–246. [[CrossRef](#)]
21. Saïdou; Abiama, P.E.; Tokonami, S. Comparative study of natural radiation exposure to the public in three uranium and oil regions of Cameroon. *Radioprotection* **2015**, *50*, 265–271. [[CrossRef](#)]
22. Jiomeneck, P.S.T.; Tematio, P.; Wilson, M.A.; Yemefack, M. Andosolization of Soils on a Strombolian Cone at Mount Bambouto, Cameroon. *Open J. Soil Sci.* **2011**, *1*, 97–105. [[CrossRef](#)]
23. Tedonkeng, P.E. Rainfall Variability along the Southern Flank of the Bambouto Mountain (West-Cameroon). *J. Cameroon Acad. Sci.* **2008**, *8*, 45–52.
24. Tematio, P.; Kengni, L.; Bitom, D.; Hodson, M.; Fopoussi, J.; Leumbe, O.; Mpakam, H.; Tsozué, D. Soils and their distribution on Bambouto volcanic mountain, West Cameroon highland, Central Africa. *J. Afr. Earth Sci.* **2004**, *39*, 447–457. [[CrossRef](#)]
25. Kenfack, P.L.; Tematio, P.; Kwekam, M.; Ngueutchoua, G.; Njike, P.R. Evidence of a Miocene volcano-sedimentary lithostratigraphic sequence at Ngwa (Dschang Region, West Cameroon): Preliminary analyses and geodynamic interpretation. *J. Pet. Technol. Altern. Fuels.* 2011, 2, pp. 25–34. Available online: <http://www.academicjournals.org/JPTAF> (accessed on 1 September 2022).

26. Dongmo, F.W.N.; Yongue, R.F.; Bolarinwa, A.T.; Ngatcha, R.B.; Fuanya, C.; Kamga, M.A. *Contribution to the Study of Bauxites' Formation in the Fongo-Tongo (Western Cameroon) Sites*; Springer International Publishing: Cham, Switzerland, 2019; pp. 241–244. [[CrossRef](#)]
27. Dongmo, F.W.N.; Fouateu, R.Y.; Ntuala, R.F.D.; Lemdjou, Y.B.; Ledoux, D.C.; Bolarinwa, A.T. Geochemical, mineralogical and macroscopic facies of the Fongo-Tongo bauxite deposit western Cameroon. *Appl. Earth Sci. Trans. Inst. Min. Metall.* **2021**, *130*, 23–41. [[CrossRef](#)]
28. Tchamba, A.B.; Yongue, R.; Melo, U.C.; Kamseu, E.; Njoya, D. Caractérisation de la bauxite de HaléoDanielle (MinimMartap, Cameroun) en vue de son utilisation industrielle dans les matériaux à haute teneur en alumine. *Silic. Ind.* **2008**, *73*, 77–84.
29. Mehra, R.; Sonkawade, R.G.; Badhan, K.; Singh, S. Measurement of natural radioactivity in rock samples using gamma ray spectrometry. *Asian J. Chem.* **2009**, *21*, 212–215. [[CrossRef](#)]
30. Livens, F. Measurement of radionuclides in food and the environment. *A guidebook. J. Environ. Radioact.* **1990**, *11*, 201–202. [[CrossRef](#)]
31. Ademola, A.K.; Bello, A.K.; Adejumobi, A.C. Determination of natural radioactivity and hazard in soil samples in and around gold mining area in Itaganmodi, south-western, Nigeria. *J. Radiat. Res. Appl. Sci.* **2014**, *7*, 249–255. [[CrossRef](#)]
32. Mbonu, C.C.; Essiett, A.A.; Ben, U.C. Geospatial assessment of radiation hazard indices in soil samples from Njaba, Imo State, South-Eastern Nigeria. *Environ. Challenges* **2021**, *4*, 100117. [[CrossRef](#)]
33. Mirion Technologies (Canberra). Genie TM 2000 Software, Basic Spectroscopy. 2016. Available online: <https://www.google.com/url?sa=t&rct=j&q=&esrc=s&source=web&cd=&cad=rja&uact=8&ved=2ahUKEwirucvf0qb7AhUUEVvkFHczAD-gQFnoECAoQAQ&url=https%3A%2F%2Fwww3.nd.edu%2F~{}wzech%2FGenie%25202000%2520Operations%2520Manual.pdf&usg=AOvVaw0a4Hg7xAEMTZPukRCd3oLp> (accessed on 23 September 2022).
34. Bineng, G.S.; Hosoda, M.; Siaka, Y.F.T.; Akata, N.; Talla, S.F.; Abiama, P.E.; Tokonami, S. External radiation exposure to the public using car-borne survey method in the uranium and thorium bearing region of Lolodorf, Cameroon External Radiation Exposure to the Public Using Car-borne Survey Method in the Uranium and Thorium Bearing Region of L. *Radiat. Environ. Med.* **2020**, *9*, 13–20.
35. Bobbo, M.O.; Saïdou, I.; J.E.N.N.; Suzuki, T.; Kudo, H.; Hosoda, M.; Owono, L.C.O.; Tokonami, S. Occupational Natural Radiation Exposure at the Uranium Deposit of Kitongo, Cameroon. *Radioisotopes* **2019**, *68*, 621–630. [[CrossRef](#)]
36. Shouop, C.J.G.; Moyo, M.N.; Chene, G.; Mekontso, E.J.N.; Motapon, O.; Kayo, S.A.; Strivay, D. Assessment of natural radioactivity and associated radiation hazards in sand building material used in Douala Littoral Region of Cameroon, using gamma spectrometry. *Environ. Earth Sci.* **2017**, *76*, 164. [[CrossRef](#)]
37. Raghu, Y.; Ravisankar, R.; Chandrasekaran, A.; Vijayagopal, P.; Venkatraman, B. Assessment of natural radioactivity and radiological hazards in building materials used in the Tiruvannamalai District, Tamilnadu, India, using a statistical approach. *J. Taibah Univ. Sci.* **2017**, *11*, 523–533. [[CrossRef](#)]
38. SARAD GmbH. Nuc Scout, Portable Gamma Identifier—Quantifier—Dose Rate Meter. 2018. Available online: www.sarad.de/info@sarad.de (accessed on 8 September 2022).
39. SARAD GmbH. Manual Software dVISION. Wiesbadener Straße 10 D-01159 Dresden Germany. 2015. Available online: https://www.sarad.de/cms/media/docs/handbuch/Manual_dVISION_EN_16-10-15.pdf (accessed on 8 September 2022).
40. SARAD GmbH. Manual Software dCONFIG. Wiesbadener Straße 10 D-01159 Dresden DEUTSCHLAND. 2009. Available online: http://www.sarad.de/cms/media/docs/handbuch/Manual_dCONFIG_EN_21-12-12.pdf (accessed on 8 September 2022).
41. Gammadata. *User's Guide MARKUS 10 The Instrument for Determining the Radon Content in the Soil*; Gammadata: Uppsala, Sweden, 2019.
42. Agbalagba, E.; Avwiri, G.; Chad-Umoreh, Y. γ -Spectroscopy measurement of natural radioactivity and assessment of radiation hazard indices in soil samples from oil fields environment of Delta State, Nigeria. *J. Environ. Radioact.* **2012**, *109*, 64–70. [[CrossRef](#)] [[PubMed](#)]
43. Soh, S.T.; Saïdou, Hosoda, M.; Ii, J.N.N.; Akata, N.; Bouba, O.; Tokonami, S. Natural radioactivity measurements and external dose estimation by car-borne survey in Douala city, Cameroon. *Radioprotection* **2018**, *53*, 255–263. [[CrossRef](#)]
44. Penabei, S.; Bongue, D.; Maleka, P.; Dlamini, T.; Saïdou; Shouop, C.G.; Halawlaw, Y.; Ebongue, A.N.; Njock, M.K. Assessment of natural radioactivity levels and the associated radiological hazards in some building materials from Mayo-Kebbi region. *Chad. Radioprotection* **2018**, *53*, 265–278. [[CrossRef](#)]
45. Ndontchueng, M.M.; Nguelem, E.J.M.; Motapon, O.; Njinga, R.L.; Simo, A.; Guembou, J.C.S.; Yimele, B. Radiological Hazards in Soil from the Bauxite Deposits Sites in Dschang Region of Cameroon. *Br. J. Appl. Sci. Technol.* **2015**, *5*, 342–352. [[CrossRef](#)]
46. Saleh, H.; Abu Shayeb, M. Natural radioactivity distribution of southern part of Jordan (Ma'an) Soil. *Ann. Nucl. Energy* **2014**, *65*, 184–189. [[CrossRef](#)]
47. Pisapak, P.; Todorovic, N.; Bhongsuwan, T. Correlation between radon and radium concentrations in soil and estimation of natural radiation hazards in Namom district, Songkhla province (Southern Thailand). *Environ. Earth Sci.* **2017**, *76*, 139. [[CrossRef](#)]
48. Yu, C.; Zielen, A.J.; Cheng, J.J.; LePoire, D.J.; Gnanapragasam, E.; Kamboj, S.; Arnish, J.; Wallo, A., III; Williams, W.A. *User's Manual for RESRAD Version 6*; Environmental Assessment Division, Argonne National Laboratory (ANL): Lemont, IL, USA, 2001; p. 458. Available online: <http://resrad.evs.anl.gov/docs/resrad6.pdf> (accessed on 17 September 2022).
49. Orosun, M.M.; Usikalu, M.R.; Oyewumi, K.J.; Achuka, J.A. Radioactivity levels and transfer factor for granite mining field in Asa, North-central Nigeria. *Heliyon* **2020**, *6*, e04240. [[CrossRef](#)]

50. European Commission. *Report on Radiological Protection Principles Concerning the Natural Radioactivity of Building Materials, Radiation Protection No. 112. Directorate-General Environment, Nuclear Safety and Civil Protection*; European Commission: Brussels, Belgium, 1999.
51. Aladeniyi, K.; Olowookere, C.; Oladele, B.B. Measurement of natural radioactivity and radiological hazard evaluation in the soil samples collected from Owo, Ondo State, Nigeria. *J. Radiat. Res. Appl. Sci.* **2019**, *12*, 200–209. [[CrossRef](#)]
52. Darwish, D.; Abul-Nasr, K.; El-Khayatt, A. The assessment of natural radioactivity and its associated radiological hazards and dose parameters in granite samples from South Sinai, Egypt. *J. Radiat. Res. Appl. Sci.* **2015**, *8*, 17–25. [[CrossRef](#)]
53. Hiéronymus, B. Etude minéralogique et géochimique des formations bauxitiques de l'Ouest du Cameroun. *Cah. ORSTOM Sér. Géologie* **1973**, *5*, 97–112.
54. Curien, H. *La Radioactivité des Roches, par R. Coppens, Collection « Que Sais-Je ? » N°741, 1957*; Presses Universitaires de France: Paris, France, 1957; Volume 1.
55. Waterways, I.N. *Sediments and pollution General Considerations*; IAEA: Vienna, Austria, 1984; p. 33.
56. Boukhenfouf, W.; Boucenna, A. The radioactivity measurements in soils and fertilizers using gamma spectrometry technique. *J. Environ. Radioact.* **2011**, *102*, 336–339. [[CrossRef](#)] [[PubMed](#)]
57. Ngachin, M.; Garavaglia, M.; Giovani, C.; Njock, M.K.; Nourreddine, A. Radioactivity level and soil radon measurement of a volcanic area in Cameroon. *J. Environ. Radioact.* **2008**, *99*, 1056–1060. [[CrossRef](#)] [[PubMed](#)]
58. Nguelem, E.; Ndontchueng, M.M.; Motapon, O.; Darko, E.O.; Simo, A. Determination of ^{226}Ra , ^{232}Th , ^{40}K and ^{235}U in soil samples from bauxite core deposits in western Cameroon. *Radioprotection* **2016**, *51*, 199–205. [[CrossRef](#)]
59. Esan, D.T.; Sridhar, M.K.C.; Obed, R.; Ajiboye, Y.; Afolabi, O.; Olubodun, B.; Oni, O.M. Determination of Residential Soil Gas Radon Risk Indices Over the Lithological Units of a Southwestern Nigeria University. *Sci. Rep.* **2020**, *10*, 7368. [[CrossRef](#)]
60. Merdanoğlu, B.; Altınsoy, N. Radioactivity concentrations and dose assessment for soil samples from Kestanbol granite area, Turkey. *Radiat. Prot. Dosim.* **2006**, *121*, 399–405. [[CrossRef](#)]
61. Sannappa, J.; Ningappa, C.; Narasimha, K.N.P. Natural radioactivity levels in granite regions of Karnataka State. *Indian J. Pure Appl. Phys.* **2010**, *48*, 817–819.
62. Nguyen, P.T.H.; Nguyen, V.T.; Vu, N.B.; Le Cong, H. Soil radon gas in some soil types in the rainy season in Ho Chi Minh City. *Vietnam. J. Environ. Radioact.* **2018**, *193–194*, 27–35. [[CrossRef](#)]
63. Yalim, H.A.; Akkurt, I.; Ozdemir, F.B.; Unal, R.; Sandikcioglu, A.; Akkurt, A. The Measurement of Radon and Radium Concentrations in Well Water in the Afyonkarahisar area of Turkey. *Indoor Built Environ.* **2007**, *16*, 77–81. [[CrossRef](#)]
64. Petropoulos, N.; Anagnostakis, M.; Simopoulos, S. Photon attenuation, natural radioactivity content and radon exhalation rate of building materials. *J. Environ. Radioact.* **2002**, *61*, 257–269. [[CrossRef](#)]
65. Souffit, G.D.; Saïdou, S.; Modibo, O.B.; Lepoire, D.; Tokonami, S. Risk Assessment of Exposure to Natural Radiation in Soil Using RESRAD-ONSITE and RESRAD-BIOTA in the Cobalt-Nickel Bearing Areas of Lomié in Eastern Cameroon. *Radiation* **2022**, *2*, 177–192. [[CrossRef](#)]
66. Ii, J.E.N.N.; Manga, A.; Saïdou, German, O.; Sainz-Fernandez, C.; Kwato Njock, M.G. Natural radioactivity in building materials, indoor radon measurements, and assessment of the associated risk indicators in some localities of the Centre Region. *Cameroon. Environ. Sci. Pollut. Res.* **2022**, *29*, 54842–54854. [[CrossRef](#)]
67. Risica, S.; Bolzan, C.; Nuccetelli, C. Radioactivity in building materials: Room model analysis and experimental methods. *Sci. Total Environ.* **2001**, *272*, 119–126. [[CrossRef](#)]
68. Souffit, G.D.; Valdes, M.J.; Modibo, O.B.; Flore, T.S.Y.; Félix, B.A.J.; Saïdou; Tokonami, S. Radon Risk Assessment and Correlation Study of Indoor Radon, Radium-226, and Radon in Soil at the Cobalt–Nickel Bearing Area of Lomié, Eastern Cameroon. *Water Air Soil Pollut.* **2022**, *233*, 196. [[CrossRef](#)]